ACS APPLIED BIO MATERIALS

Article

Multivalued logic assay of the disease marker of #-ketoglutaric acid by a luminescent MOF-based biosensor

xu dai, Jina Hao, Jinlou Gu, and Yongsheng Li

ACS Appl. Bio Mater., **Just Accepted Manuscript** • DOI: 10.1021/acsabm.0c00378 • Publication Date (Web): 17 May 2020

Multivalued logic assay of the disease marker of α-ketoglutaric acid by a luminescent MOF-based biosensor

Xu Dai, Ji-Na Hao, Jinlou Gu and Yongsheng Li**

Laboratory of Low-Dimensional Materials Chemistry, Key Laboratory for Ultrafine Materials of Ministry of Education, Shanghai Engineering Research Center of Hierarchical Nanomaterials, School of Materials Science and Engineering, East China University of Science and Technology, Shanghai 200237, P. R. China.

Corresponding author. E-mail address: haona1220@126.com; ysli@ecust.edu.cn.

ABSTRACT: α-Ketoglutaric acid (α-KA) is an important endogenous metabolite in the Krebs cycle and considered to be a critical marker of various diseases. Several approaches for identifying α-KA have been reported. However, most of them are limited to single-signal transduction modes in one assay and working in suspension state, which easily suffer from quantification errors and lead to false-positive detection results. Herein, a multivalue-responsive and semisolid EuMOF-gel (EuMOG) logic biosensor is firstly designed and fabricated, which can realize the specific, rapid, and easy-to-differentiate naked-eye detection of the disease-associated marker of α-KA in serum through implementing a one-to-two logic operation with three multicolor gates. The implementation of 1-to-2 logic operation can be rationally achieved by assembling 2,6-naphthalenedicarboxylic acid (NDC) as both the energy donor and blue-colored output 1, photoactive Eu^{3+} ions as the red-emissive output 2, and α-KA stimuli as an input and energy blocker between the two spectrum-resolved outputs, into one unit. With the specific input of α-KA among various analytes, the binary code of the logic decoder switches from (0,1) to (1,0) with an obvious color change from red to cyan. Moreover, by integrating the output chromaticity into the logical operations, the concentration levels of α-KA could be easily evaluated with the intelligent EuMOG detector, which has three multicolor gates in parallel encoding low (0,1), normal (1,1) and danger (1,0) status. Such multivalued logic biosensor provides a facile strategy to improve the analysis reliability for disease-associated biomarkers.

KEYWORDS: luminescent MOF, biosensor, multivalued logic assay, disease marker, α-ketoglutaric acid

INTRODUCTION

Preclinical diagnosis and prognosis of diseases, especially cancers, are decisive for their successful treatments, which can effectively reduce the disease mortality.[1] Since the pathogenic processes of diseases are always accompanied with the prominent alterations of specific biomolecules (recognized as disease markers), sensitive and accurate detection of these markers is essential for the diseases' early diagnosis and timely therapy.[1-3] As a diseases-related marker, α-ketoglutaric acid (α-KA) is an endogenous metabolite in the Krebs cycle catalyzed by isocitrate dehydrogenase (IDH) and occupies a central position in the energy homeostasis and cell metabolism.[4] It has been reported to be associated with the somatic mutation of IDH and a variety of metabolic disorders,[5,6] and a critical indicator for diverse diseases including diabetic II,[7] liver cancer,[7] nonalcoholic fatty liver disease,[8] polycystic kidney disease,[9] etc. Therefore, it is of vital importance to trace the abnormal expression of α-KA for monitoring the disease progression. Despite the biological importance of α-KA, it still remains a challenge to construct a simple, fast and accurate method for α-KA analysis since some traditional methods such as chromatography either require laborious pretreatment or involve time-consuming test.[10-19] In contrast, fluorescence materials provide a facile detection method for various species with several advantages of simple operation/procedure, cost-saving apparatus, rapid analysis time, and even naked-eye visibility. Nevertheless, most of the reported fluorescence platforms for α-KA suffer from a series of drawbacks including working with the assistance of extra certain surfactant (CTAB)[20,21] or in organic media,[22] requiring long reaction time[23,24] or complicated material fabrication process,[26] and relying on an enzymatic transamination.[27] Besides, a major impediment of these fluorescence probes is that they mainly depend on single-signal transduction modes that are "always on" or "always off" to assay the analyte, which are susceptible to the

instrument/environment conditions, resulting in the increase of quantification errors and false positives rate. Therefore, developing a facile, fast, multiple-channel-responsive optical probe for α-KA detection with high reliability is highly desired.

Luminescent metal-organic frameworks (LMOFs), as a subfield class of MOFs, have been proved as one of the most promising chemosensory materials owing to their intrinsic structure properties, unique luminescence features and the fruitful energy/electron transfer processes among photonic units and analytes.[28-32] Till now, much efforts have been made on developing LMOFs for detection of various analytes[33-43] and different humidity/temperature conditions,[44-50] however, few studies on exploiting such materials for detecting α-KA have been reported. More importantly, most of the reported luminescent MOF-based sensors prefer working in suspension state, which are subject to signal fluctuations due to the irregular movement of the insoluble MOF particles in the analytical sample. Herein, by assembling and solidifying the luminescent EuMOF into the agarose gel, a novel dual-channel-responsive EuMOG logic system for qualitative and quantitative analysis of α-KA in serum was developed. The implementation of 1-to-2 logic operation was rationally achieved by assembling 2,6-naphthalenedicarboxylic acid (NDC) as both the energy donor and blue-colored output 1, photoactive Eu^{3+} ions as the red-emissive output 2, and α-KA stimuli as an input and energy blocker between the two spectrum-resolved outputs, into one unit. With the specific input of α-KA among various analytes, the binary code of the logic decoder switches from (0,1) to (1,0) with an easy-to-differentiate color change from red to cyan. Moreover, by integrating the output chromaticity into the logical operation, the concentration levels of α-KA could be easily evaluated with the intelligent EuMOG detector, which has three multicolor gates in parallel encoding low (0,1), normal (1,1) and danger (1,0) status. Such logic operation of EuMOG for serum α-KA also exhibits specific,

sensitive and fast assay performances, presenting a promising platform for dual-channel analysis of biomolecules.

EXPERIMENTAL SECTION

Materials and Reagents. 2,6-Naphthalenedicarboxylic acid (98%), 4,4'-bipyridine (98%) and agarose were purchased from Aladdin and used as received without further purification. Europium nitrate hexahydrate was obtained by dissolving the corresponding oxide compounds in HNO_3 (68%) followed by evaporation and crystallization. All the other materials were commercially available reagents of analytical grade.

Synthesis of the EuMOF. A mixture of $Eu(NO_3)_3 \cdot 6H_2O$ (0.08 $mol \cdot L^{-1}$, 1.25 mL), 2,6-Naphthalenedicarboxylic acid (NDC, 0.2 mmol, 42 mg), 4,4'-bipyridine (0.06 mmol, 10 mg), DMF (4 mL), and distilled H_2O (0.75 mL) was added in a 23 mL-Teflon liner of autoclave and stirred for 30 min at room temperature. Then the Teflon liner was sealed in the stainless steel container and placed into a pre-heated oven at 60 °C for 4 days.[51] After slowly cooling down to room temperature, a white-powdered product was obtained by centrifugation, washed with water, and finally dried in air at 35 °C.

Synthesis of the EuMOG Biosensor. 2 g of agarose powder was added to 80 mL ultrapure water and heated by a water bath to 90°C until it was completely dissolved. Then, the as-prepared MOFs powder (2.5 mg) was dispersed into water (0.5 mL) under ultrasound to form an aqueous suspension, and subsequently added to the above agarose solution (2.5 mL) dropwise. After sonicating, the mixtures cooled down sufficiently until a semisolid hydrogel was formed.[37]

Procedures for α-KA Detection. In the typical and selective assay for α-KA, aqueous solutions (5×10^{-3} M, 10 mL) of α-KA and various biologically relevant species, including L-isoleucine (LLE), L-leucine (LEU), dopamine (DA), phenylglyoxal (PGO), L-threonine (THR),

sodium pyruvate (PAS), L-proline (PRO), L-tryptophan (TRP), L-serine (SER), glucose (GLC), H_2O_2, KCl and NaCl, were incubated with the EuMOG samples (3 mL) for 20 min, respectively. Then the luminescence spectra of the analytes-impregnated EuMOGs were measured and recorded under excitation of 350 nm, and the digital photos were taken under irradiation of a 365 nm-UV lamp. Test samples for the quantitative experiment were prepared with a similar procedure. The standard addition technique was used for the determination of α-KA in the fetal bovine serum samples diluted with 60-fold deionized water.

Instruments and Characterizations. The powder X-Ray diffraction (PXRD) patterns were collected on a Bruker D8 instrument using Cu Kα radiation (40kV, 40mA) at a scanning rate of $8°\cdot min^{-1}$. Field emission scanning electron microscopy (FESEM) and energy dispersive X-ray (EDX) spectroscopy mapping was determined by a GeminiSEM500 electron microscope. The excitation/emission spectra were measured on a RF-5301PC spectrophotometer (Shimadzu). The lifetime decays were recorded on an Edinburgh FLS920 fluorescence spectrophotometer equipped with pulsed flash lamps. All digital photographs were taken by a cellphone.

RESULTS AND DISCUSSION

Characterization of the EuMOG Biosensor. The synthesis process of the EuMOG is presented in Figure 1a. Initially, the pristine EuMOF was synthesized via the solvothermal reaction of $Eu(NO_3)_3$ with the ligands of NDC and 4,4'-bipyridine. PXRD shows that the diffraction peaks of the experimental EuMOF match well with that of the simulated one (Figure 1b),[51] indicating the high crystalline-phase purity of the as-synthesized EuMOF. The stability of the EuMOF was then examined by soaking it in water for 24 h (Figure S1). It is observed that the EuMOF maintained high crystallinity after treated with water, suggesting that it is qualified to be

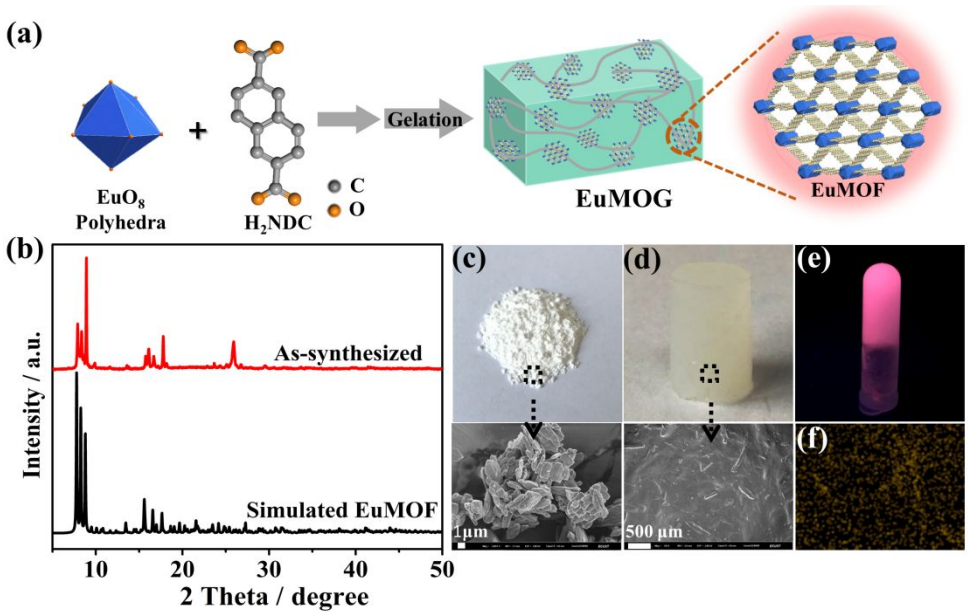

Figure 1. (a) Illustration for the synthesis process of the EuMOG composite; (b) PXRD patterns of the simulated and as-synthesized EuMOF; (c,d) Digital photos and the corresponding SEM images of EuMOF powder (c) and EuMOG (d); (e) Photograph of the EuMOG in tube under a 365 nm UV-light irradiation; (f) Elemental mapping images of Eu in the freeze-dried EuMOG sample.

embedded into the hydrogels matrix and applied in the aqueous medium. Subsequently, the EuMOF powder was dispersed into the aqueous solution of agarose, yielding the EuMOF-integrated hydrogel (denoted as EuMOG) after cooling (Figure 1d). SEM image (Figure 1d) of the freeze-dried EuMOG indicates the presence of the MOF particles throughout the gel body, and the EDX mapping analysis reveals an even distribution of Eu element in the composite (Figure 1f). After the successful synthesis of the EuMOG, its photoluminescence properties were then investigated. As shown in Figure S2a, the excitation spectrum of the EuMOG monitored at the characteristic emission (615 nm) of the Eu^{3+} exhibits a broad band with a maximum absorption at 350 nm, which arises from the NDC electron transitions. When excited at 350 nm,

the NDC-centered broad emission of the EuMOG ranging from 400 to 560 nm is rather weak, while the Eu^{3+} ions' well-resolved characteristic emissions (579, 592, 615, 652, and 697 nm) of $^5D_0 \rightarrow {}^7F_J$ (J = 0 - 4) transitions are highly intense. This demonstrates the high efficiency of NDC-to-Eu^{3+} energy transfer in the EuMOG, resulting in an obvious red-color output that is visible to the naked eyes under a 365 nm-UV light (Figure 1e). Compared with the EuMOF aqueous suspension (Figure S2b), the relative emissions of the ligand and Eu^{3+} in the EuMOG almost have no change, which indicates the introduction of agarose hardly affect the EuMOF's luminescence. Moreover, the EuMOG's dual-emission signals have almost no fluctuations during the 3 days' storage (Figure S3), verifying its high luminescence stability and the good immobilization of the EuMOF powder by the gel. Such excellent luminescence performances are expected to provide advantages for reliable analysis of the bio-targets.

Logic Assay Properties of the Dual-Channel Biosensor for α-KA. The pH-dependent optical property of EuMOG in the range of 4.0-8.0 was examined. The results in Figure S4 show that its emission behavior is insusceptible to pH within the physiological range. The responsive performance of EuMOG towards α-KA was then evaluated. As shown in Figure 2a and b, with the presence of α-KA, the red emission of Eu^{3+} at 615 nm (R2) was significantly decreased by 90.5%, while the blue-colored signal (B1) of NDC centered at 460 nm became apparent. As a result, the B1/R2 intensity ratio (I_1/I_2) of the α-KA-impregnated EuMOG exhibits a remarkable 63.5-fold enhancement, compared with that of the blank EuMOG, triggering an obvious and visible output transition from red to cyan color under a 365 nm-UV lamp. These suggest that EuMOG can function as a dual-channel signal transducer for single α-KA with "turn-on" response of B1 and "turn-off" response of R2, establishing a one-to-two logic decoder (Figure 2c). In the logic operation process, the fabricated EuMOG behaves as a gate, the α-KA bio-target

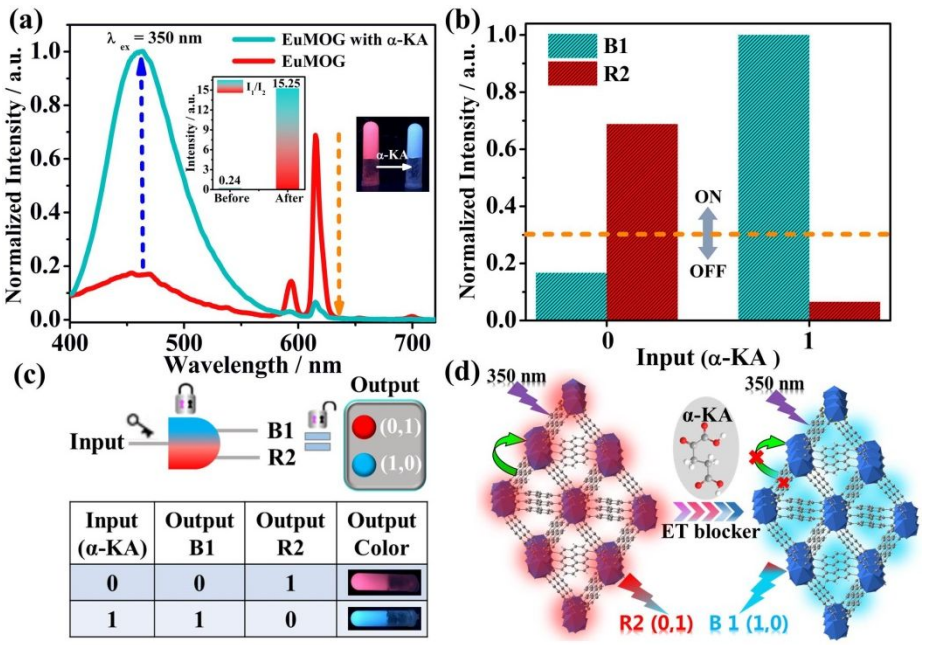

Input (α-KA)	Output B1	Output R2	Output Color
0	0	1	
1	1	0	

Figure 2. (a) Emission spectra and normalized intensities (b, threshold: 0.3) of EuMOG before and after treated with α-KA (5×10^{-3} M). Inset: intensity ratio changes of the two outputs, and color variation of EuMOG with a 365-UV lamp; (c) Truth table of the 1-to-2 logic gate; (d) Schematic of luminescence response mechanism of EuMOG towards α-KA.

is used as an input, and the emission signals of B1 and R2 emitters are taken as output 1 and output 2, respectively. The presence and absence of input are defined as "1" and "0" states, respectively. The normalized fluorescence intensities of the two outputs are translated into binary "0" (below) or "1" (above) by comparing them with the threshold value of 0.3. As shown in the truth table (Figure 2c), in the absence of α-KA (input = 0), the double responsive signals give an output of (0,1). With the input of α-KA (input = 1), the B1 signal changes from off to on while the R2 signal switches from on to off, generating an output of (1,0). Such opposite responsive behaviors of the two outputs in EuMOG biosensor can be ascribed to the fact that the presence of α-KA blocks the energy transfer from NDC to Eu^{3+} through bonding destruction[52,53], as demonstrated by the PXRD (Figure S5) and the decreased lifetime of Eu^{3+} (Figure S6), leading

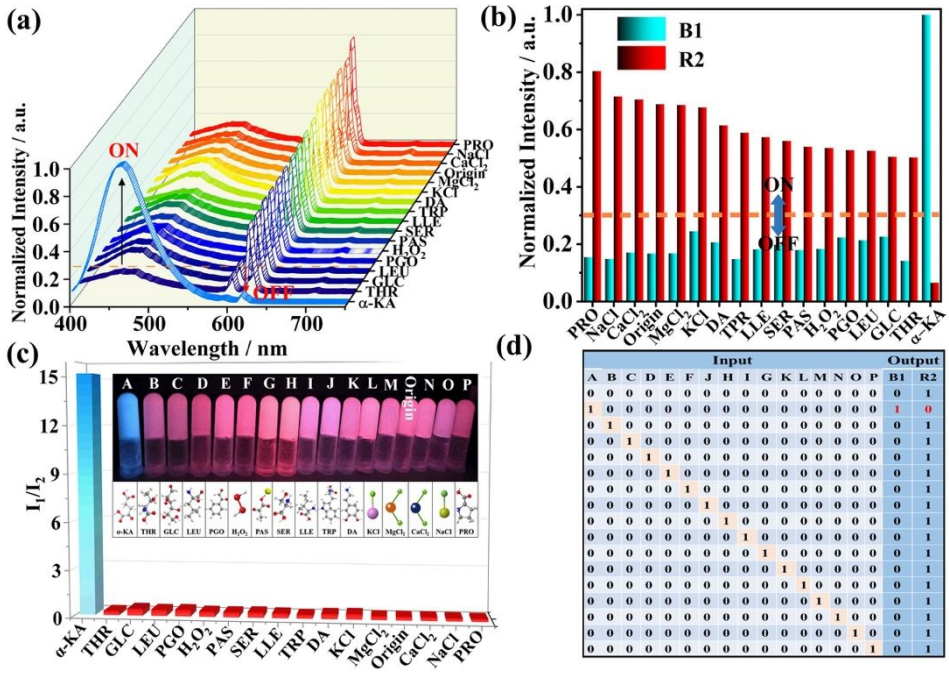

Figure 3. The fluorescence spectra (a), the normalized intensities of B1, R2 (b, threshold: 0.3), and the B1/R2 intensity ratio (c) of EuMOG towards biologically interfering species. Inset in (c): Digital photos of EuMOG responding to various species under a 365 nm UV lamp; (d) Truth table of the logic EuMOG with different components as inputs.

to the self-dominated luminescence of the NDC energy donor (Figure 2d and S7). These demonstrate the logic dual-channel analysis ability of EuMOG for α-KA. Notably, such logic operation for α-KA was completed by EuMOG within 20 min, as demonstrated in Figure S8, which shows that the intensity (I_1/I_2) change of the two outputs reach equilibrium at the reaction time of 20 min.

In order to examine the selectivity of the logic bioprobe for α-KA, the luminescence behaviors of the EuMOG incubated with various typical species in serum were investigated. As shown in Figure 3a-c, the signal intensity changes of the EuMOG treated with various potential interferents in serum are much smaller than that with α-KA, and nearly similar to the free

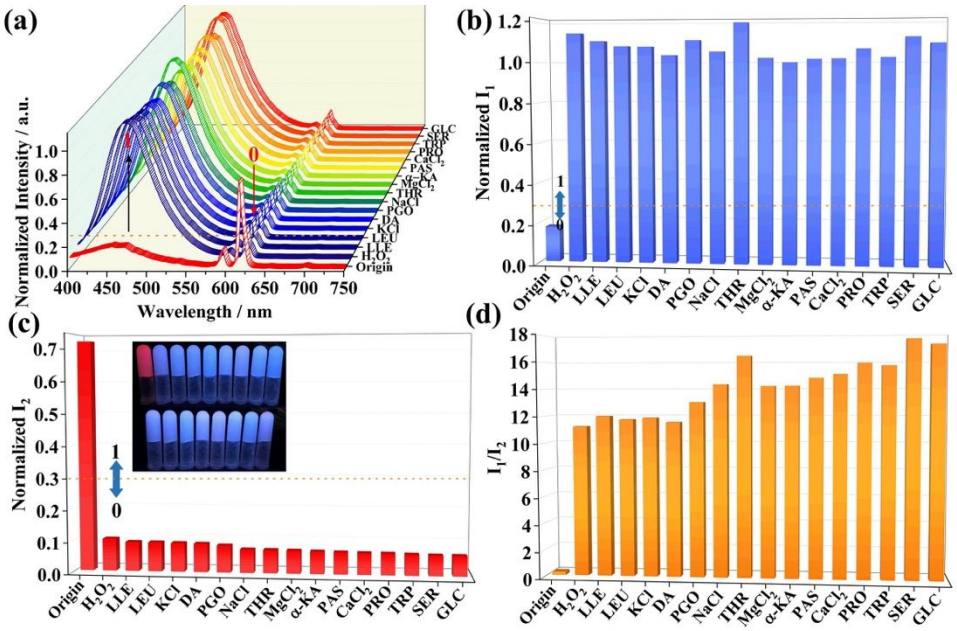

Figure 4. Luminescence spectra (a) and column diagrams of the normalized fluorescence intensities (b, I_1; c, I_2; d, I_1/I_2) of EuMOG towards α-KA in the presence of other various species (λ_{ex} = 350 nm).

EuMOG. As a result, only the input of α-KA induces the dual outputs to switch from (0,1) to (1,0), accompanying with an easy-to-distinguish color transition from red to cyan under a UV lamp irradiation, while all the other inputs induce the EuMOG transducer to export the original output of (0,1) without any color transitions (Figure 3d). Such high selectivity of the EuMOG allows it for logic and visual assay of α-KA over various species. This probably originates from the fact that only α-KA among various analytes interrupts the coordination bonds between B1 and R2 outputs and thus hinders the B1-to-R2 energy transfer. Moreover, when α-KA and the interferents are simultaneously input in the system, both the response efficiency (I_1, I_2 and I_1/I_2) and color transitions of the EuMOG exhibit similar variations with that using α-KA as the single input (Figure 4), and all the outputs of EuMOG with the other fifteen combinatorial inputs exhibit "(1,0)" state with cyan emission colors (Figure S9), demonstrating that the presences of

these interferents have negligible influences on the analysis of α-KA by the EuMOG logic system. These indicate that the EuMOG has outstanding specificity for discriminating α-KA from various coexisting analytes in mimic serum.

The concentration-dependent photo-luminescence of the EuMOG towards α-KA was measured to investigate its quantitative assay ability (Figure 5a). It is observed that the EuMOG's emission intensity of B1 was progressively enhanced, while that of R2 was gradually decreased with the incremental α-KA concentration (0 - 5×10^{-3} M), resulting in the gradual shift of CIE coordinates from (0.4377, 0.2776) to (0.1665, 0.1748) and the color change from red to faint, and to cyan under a 365 nm UV lamp (Figure 5b). On the basis of ratiometric chromaticity and color transitions, four concentration ranges were divided and set as the input signals, and thus a one-to-two decoder with three gates of YES (0,1), OK (1,1) and NO (1,0) was constructed to reflect the α-KA levels. As shown in Figure 5c, when the concentration of α-KA is below than 10^{-4} M, the signal intensity of output B1 is lower than that of output R2, and the YES gate encoding (0,1) appears with red/purplish-red light on. When the concentration is in the range of 1×10^{-4} M to 7×10^{-4} M, the OK (1,1) gate is triggered to be unlocked by α-KA within this content range, and presents a faint light, indicating the normal level of α-KA. Once the input of α-KA is higher than 7×10^{-4} M, the B1 signal of the logic EuMOG becomes weaker than R2, and the NO gate with encode of (1,0) and the cyan alarm lamp are switched on, reminding us of the abnormal and high level of α-KA, as the critical value of α-KA concentration in healthy human is 7.3×10^{-4} M.[7] By connecting the color-coded light and logical operations to the analysis, the EuMOG's detection signals for α-KA levels were converted into simple binary computer language, in which the outputs of (0,1), (1,1), and (1,0) encode low, normal, and danger level of α-KA, respectively. Hence, this EuMOG logic biosensor provides a predictive algorithm for α-KA level, making it

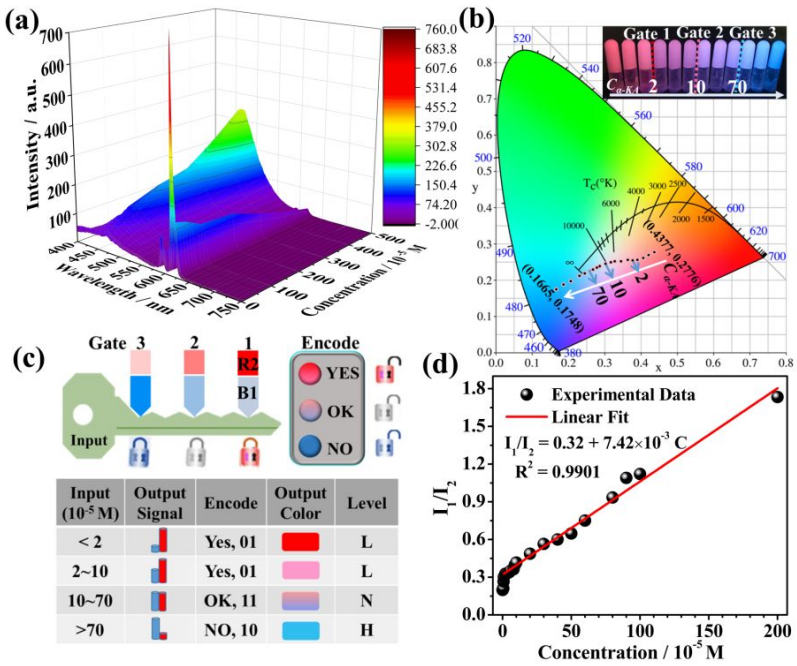

Figure 5. Luminescence responses (a) and CIE chromaticity coordinates (b) of EuMOG to different concentrations of α-KA ranging from 0 to 5×10^{-3} M; Inset in (b): Color changes of EuMOG with increasing α-KA concentration under irradiation of a 365nm-UV lamp; (c) Scheme and table for the logic operation of EuMOG with three gates for visually decoding α-KA level (L: low, N: normal, H: high); (d) Linear fitted curve of I_1/I_2 *vs.* $C_{\alpha\text{-KA}}$.

possible to develop an artificial intelligence (AI) early warning system for people to understand their health status.

For more accurate quantification of the α-KA concentration, the dependence of the B1/R2 intensity ratio of EuMOG on the α-KA concentration was plotted and fitted. As shown in Figure 5d, there is a good linear relationship ($R^2 = 0.9901$) between the response signal (I_1/I_2) and α-KA concentration ranging from 10^{-5} to 2×10^{-3} M, which can be fitted as a function of Equation (1).

$$I_1/I_2 = 0.32 + 7.42\times10^{-3}\, C_{\alpha\text{-KA}} \quad (1)$$

The limit of detection (LOD) is calculated to be 6.87 μM by the 3σ/slope (δ, the standard deviation of the intensity of blank sample for ten times),[54] which is markedly lower than the

danger level of 7.3×10^{-4} M for people.[7] Both the low LOD and the linear detection range enable this dual-channel logic system to sensitively and quantitatively detect α-KA within physiologically relevant ranges. Compared with the previously reported methods (Table S1), the LOD of the EuMOG are lower than most of those detection systems. Moreover, most of those systems are subject to a single-output transduction mode in the solution state, and involve tedious synthesis/analysis processes. By contrast, our proposed approach based on the EuMOG provides a dual-channel logic assay with simple preparation and efficient analysis in the semisolid state, enabling it to be a more precise, portable and convenient device for analysis of α-KA biotarget.

Determination of α-KA in Serum. The feasibility of the EuMOG biosensor to detect α-KA in real biological matrices was explored. The diluted fetal bovine serum (FBS) spiked with α-KA at different concentrations were prepared and incubated with the EuMOG, respectively. The analyzed results (Table 1) shows that the recoveries for the α-KA measurement in three spiked serum samples range from 92.6% to 103.4% with the relative standard derivations (RSD, $n = 6$) less than 2.77 %, which well satisfy the criteria (recoveries, 90 − 110%, RSD $\leqslant$ 15%) set for the bioanalytical method validation.[55] This indicates the dual-channel responsive EuMOG biosensor has good accuracy and reliability for quantifying the α-KA in real serum samples, and possesses great application potential for early clinical diagnosis of various diseases.

Table 1. Determination of α-KA in the diluted serum samples according to the proposed approach.

Serum Samples	Spiked (10^{-5} M)	Measured (10^{-5} M, $n = 6$)	Recovery (%)	RSD (%, $n = 6$)
1	5.0	4.7 ± 0.13	94.0	2.77
2	50.0	46.3 ± 0.75	92.6	1.62
3	100.0	103.4 ± 1.50	103.4	1.45

CONCLUSIONS

In summary, a novel luminescent dual-channel-responsive EuMOG logic biosensor has been designed and fabricated for the disease-related marker (α-KA) in serum by integrating NDC as both energy donors and blue-emissive output 1 and Eu^{3+} as red-colored output 2 in a framework. By regulating the energy transfer between the dual spectrum-resolved outputs through the specific α-KA input, a one-to-two logic operation in the EuMOG was performed with the output signal switching from (0,1) to (1,0) and the output color changing from red to cyan. Significantly, by combining the ratiometric chromaticity transition with logical operations, three multicolor gates of YES (0,1), OK (1,1), and NO (1,0) were set on the EuMOG logic biosensor to encode the low/normal/danger levels of α-KA marker, allowing for its intelligent and visual evaluation of health status. Such logic system also exhibits rapid response (20 min), high sensitivity (LOD, 6.87 μM), and easy-to-differentiate naked-eye detection for α-KA without interference by other coexisting species in serum. Compared to the single-output and suspension-state fluorescence detection systems for α-KA, this multivalued-output and semisolid system can improve the analysis ability and reliability for α-KA, providing a facile strategy to design luminescent MOF-based intelligent platform for disease diagnosis.

ASSOCIATED CONTENT

Supporting Information.

PXRD patterns, luminescence spectra and decay curves, and several metrics for evaluating sensing capabilities involving water tolerance, pH tolerance, luminescence stability and anti-interference performance.

AUTHOR INFORMATION

Corresponding Author

*E-mail: haona1220@126.com

*E-mail: ysli@ecust.edu.cn

Notes

The authors declare no competing financial interest.

ACKNOWLEDGMENT

This work was financially supported by the National Key Research and Development Program of China (Grant No. 2018YFC1105702), the National Natural Science Foundation of China (Grant Nos. 51621002, 21805087 and 51972112), Shanghai Sailing Program (18YF1405900), China Postdoctoral Science Foundation (2017M621383), Program of Shanghai Academic/Technology Research Leader (18XD1401400), Basic Research Program of Shanghai (17JC1404702), Leading Talents in Shanghai in 2018, The 111 project (B14018), and the Fundamental Research Funds for Central Universities (222201718002).

REFERENCES

(1) Wu, L.; Qu, X. G. Cancer biomarker detection: recent achievements and challenges. *Chem. Soc. Rev.* **2015**, *44*, 2963-2997.

(2) Chen, Z.; Zheng, W.; Huang, P.; Tu, D.; Zhou, S.; Huang, M.; Chen, X. Lanthanide-doped luminescent nano-bioprobes for the detection of tumor markers. *Nanoscale* **2015**, *7*, 4274-4290.

(3) He, X. P.; Hu, X. L.; James, T. D.; Yoon, J.; Tian, H. Multiplexed photoluminescent sensors: towards improved disease diagnostics. *Chem. Soc. Rev.* **2017**, *46*, 6687-6696.

(4) He, W. H.; Miao, F. J.; Lin, D. C.; Schwandner, R. T.; Wang, Z. L.; Gao, J. H.; Chen, J. L.; Tian, H.; Ling, L. Citric acid cycle intermediates as ligands for orphan G-protein-coupled receptors *Nature* **2004**, *429*, 188-193.

(5) Parsons, D. W.; Jones, S.; Zhang, X. S.; Lin, J. C.; Leary, R. J.; Angenendt, P.; Mankoo, P.; Carter, H.; Siu, I.; Gallia, G. L. An integrated genomic analysis of human glioblastoma multiforme. *Science* **2008**, *321*, 1807-1812.

(6) Wu, F. R.; Jiang, H.; Zheng, B. S.; Kogiso, M.; Yao, Y.; Zhou, C.; Li, X. N.; Song, Y. C. Inhibition of cancer-associated mutant isocitrate dehydrogenases by 2-thiohydantoin compounds. *J. Med. Chem.* **2015**, *58*, 6899-6908.

(7) Makahleh, A.; Ben-Hander, G. M.; Saad, B. Determination of α-ketoglutaric and pyruvic acids in urine as potential biomarkers for diabetic II and liver cancer. *Bioanalysis* **2015**, *7*, 713-723.

(8) Gallego, E. R.; Guirro, M.; Borrull, M. R.; Aguilera, A. H.; Casado, R. M.; Arroyo, S. F.; Debón, R. B.; Sabench, F.; Hernández, M.; Castillo, D. D. Mapping of the circulating metabolome reveals α-ketoglutarate as a predictor of morbid obesity-associated non-alcoholic fatty liver disease. *Int. J. Obes.* **2015**, *39*, 279-287.

(9) Abbiss, H.; Maker, G. L.; Gummer, J.; Sharman, M. J.; Phillips, J. K.; Boyce, M.; Trengove, R. D. Development of a non-targeted metabolomics method to investigate urine in a rat model of polycystic kidney disease. *Nephrology* **2012**, *17*, 104-110.

(10) Laplante, A.; Comte, B.; Desrosiers, C. Assay of blood and tissue oxaloacetate and α-ketoglutarate by isotope dilution gas chromatography-mass spectrometry. *Anal. Biochem.* **1995**, *224*, 580-587.

(11) Wagner, B. M.; Donnarumma, F.; Wintersteiger, R.; Windischhofer, W.; Leis, H. J. Simultaneous quantitative determination of α-ketoglutaric acid and 5-hydroxymethylfurfural in human plasma by gas chromatography–mass spectrometry. *Anal. Bioanal. Chem.* **2010**, *396*, 2629-2637.

(12) Magiera, S.; Baranowska, I.; Kusa, J.; Baranowski, J. A liquid chromatography and tandem mass spectrometry method for the determination of potential biomarkers of cardiovascular disease. *J. Chromatogr. B* **2013**, *919*, 20-29.

(13) Sriboonvorakul, N.; Leepipatpiboon, N.; Dondorp, A. M.; Pouplin, T.; White, N. J.; Tarning, J.; Lindegardh, N. Liquid chromatographic–mass spectrometric method for simultaneous determination of small organic acids potentially contributing to acidosis in severe malaria. *J. Chromatogr. B* **2013**, *941*, 116-122.

(14) Donnarumma, F.; Wintersteiger, R.; Schober, M.; Greilberger, J.; Matzi, V.; Maier, A.; Schwarz, M.; Ortner, A. Simultaneous quantitation of alpha-ketoglutaric acid and 5-hydroxymethylfurfural in plasma by HPLC with UV and fluorescence detection. *Anal. Sci.* **2013**, *29*, 1177-1182.

(15) Petucci, C.; Zelenin, A.; Culver, J. A.; Gabriel, M.; Kirkbride, K.; Christison, T. T.; Gardell, S. J. Use of ion chromatography/mass spectrometry for targeted metabolite profiling of polar organic acids. *Anal. Chem.* **2016**, *88*, 11799-11803.

(16) Montenegro, P.; Valente, I. M.; Goncalves, L. M.; Rodrigues, J. A.; Barros,A. A. Single determination of α-ketoglutaric acid and pyruvic acid in beer by HPLC with UV detection. *Anal. Methods* **2011**, *3*, 1207-1212.

(17) Chen, S. S.; Burton, C.; Kaczmarek, A.; Shi, H. L.; Ma, Y. F. Simultaneous determination of urinary quinolinate, gentisate, 4-hydroxybenzoate, and α-ketoglutarate by high-performance liquid chromatography-tandem mass spectrometry. *Anal. Methods* **2015**, *7*, 6572-6578.

(18) Niu, H. Q.; Chen, Y.; Xie, J. J.; Chen, X. C.; Bai, J. X.; Wu, J. L.; Liu, D.; Ying, H. J. Ion-exclusion chromatography determination of organic acid in uridine 5'-monophosphate fermentation broth. *J. Chromatogr. Sci.* **2012**, *50*, 709-713.

(19) Fujima, J. M.; Danielson, N. D. Enzymatic amplification by substrate recycling for α-ketoglutarate in conjunction with capillary electrophoresis. *Journal of Capillary Electrophoresis and Microchip Technology* **2002**, *7*, 19-22.

(20) Jin, P. W.; Jiao, C. H.; Guo, Z. Q.; He, Y.; Zhu, S. Q.; Tian, H.; Zhu, W. H. Rational design of a turn-on fluorescent sensor for α-ketoglutaric acid in a microfluidic chip. *Chem. Sci.* **2014**, *5*, 4012-4016.

(21) He, Y.; Guo, Z. Q.; Jin, P. W.; Jiao, C. H.; Tian, H.; Zhu, W. H. Optimizing the chemical recognition process of a fluorescent chemosensor for α-ketoglutarate. *Ind. Eng. Chem. Res.* **2015**, *54*, 2886-2893.

(22) Gan, L. L.; Chen, L. H.; Nan, F. J. Discovery of a novel calcium-sensitive fluorescent probe for α-ketoglutarate. *Acta. Pharmacol. Sin.* **2017**, *38*, 1683-1690.

(23) Fu, Q.; Chen, Z.; Ma, X. Y.; Chen, G.; Liu, Y. X.; Cao, Z. P.; Qu, F.; Yang, D. S.; Zhao, X. E.; Sun, Z. W.; Li, G. L.; Zhang, S. J.; Qu, F. L.; Kong, R. M.; Wang, H. and You, J. M. Simultaneous absorbance-ratiometric, fluorimetric, and colorimetric analysis and biological imaging of α-ketoglutaric acid based on a special sensing mechanism. *Sensor Actuat. B-Chem*. **2017**, *241*, 1035-1042.

(24) Virel, A.; Sanchez-Lopez, J.; Saa, L.; Garcia, A. C.; Pavlov, V. Use of an Osmium Complex as a Universal Luminescent Probe for Enzymatic Reactions. *Chem-Eur. J.* **2009**, *15*, 6194-6198.

(25) Zhang, C.; Ye, B. C. A single fluorescent protein-based sensor for in vivo 2-oxogluatarate detection in cell. *Biosens. Bioelectron.* **2014**, *54*, 15-19.

(26) Zhan, C.; Zhang, G. X.; Zhang, D. Q. A fluorescence 'turn-on' detection of α-ketoglutaric acid with silole as the fluorescence reporter. *J. Photoch. Photobio. A.* **2018**, *355*, 366-370.

(27) Rojanarata, T.; Laiwattanapaisal, W.; Ngawhirunpat, T.; Opanasopit, P.; Worrawethanakul, K.; Chantadee, T.; Fuangwattana, T. Fast, affordable and eco-friendly enzyme kinetic method for the assay of α-ketoglutaric acid in medical product and sports supplements. *Enzyme Microb. Tech.* **2018**, *116*, 72-76.

(28) Cui, Y.; Zhang, J.; He, H.; Qian, G. Photonic functional metal–organic frameworks. *Chem. Soc. Rev.* **2018**, *47*, 5740-5785.

(29) Hao, J. N.; Xu, X. Y.; Fei, H. H.; Li, L. C.; Yan, B. Functionalization of metal–organic frameworks for photoactive materials. *Adv. Mater.* **2018**, *30*, 1705634.

(30) Wu, S.; Min, H.; Shi, W.; Cheng, P. Multicenter metal–organic framework-based ratiometric fluorescent sensors. *Adv. Mater.* **2019**, *32*, 1805871.

(31) Yan, B. Lanthanide-functionalized metal–organic framework hybrid systems to create multiple luminescent centers for chemical sensing. *Acc. Chem. Res.* **2017**, *50*, 2789-2798.

(31) Rasheed, T.; Nabeel, F. Luminescent metal-organic frameworks as potential sensory materials for various environmental toxic agents. *Coord. Chem. Rev.* **2019**, *401*, 213065-213086.

(33) Jiao, Z. H.; Jiang, X. L.; Hou, S. L.; Tang, M. H.; Zhao, B. Highly sensitive and selective luminescence sensor based on two-fold interpenetrated MOFs for detecting glutamate in serum. *Inorg. Chem.* **2020**, *59*, 2171-2177.

(34) Luo, T. Y.; Das, P.; White, D. L.; Liu, C.; Star, A.; Rosi, N. L. Luminescence "turn-On" detection of gossypol using Ln^{3+}-based metal–organic frameworks and Ln^{3+} salts. *J. Am. Chem. Soc.* **2020**, *142*, 2897-2904.

(35) Hao, J. N.; Yan, B. Determination of urinary 1-hydroxypyrene for biomonitoring of human exposure to polycyclic aromatic hydrocarbons carcinogens by a lanthanid-functionalized metal-organic framework sensor. *Adv. Funct. Mater.* **2017**, *27*, 1603856.

(36) Han, Z. S.; Wang, K.; Guo, Y.; Chen, W.; Zhang, J.; Zhang, X.; Siligardi, G.; Yang, S.; Zhou, Z.; Sun, P.; Shi, W.; Cheng, P. Cation-induced chirality in a bifunctional metal-organic framework for quantitative enantioselective recognition. *Nat. Commun.* **2019**, *10*, 5117-5123.

(37) Hao, J. N.; Li, Y. S. Concurrent modulation of competitive mechanisms to design stimuli-responsive Ln-MOFs: a light-operated dual-mode assay for oxidative DNA damage. *Adv. Funct. Mater.* **2019**, *29*, 1903058.

(38) Yang, A. F.; Hou, S. L.; Shi, Y.; Yang, G. L.; Qin, D. B.; Zhao, B. Stable lanthanide–organic framework as a luminescent probe to detect both histidine and aspartic acid in water. *Inorg. Chem.* **2019**, *58*, 6356-6362.

(39) Xu, X. Y.; Yan, B. Intelligent molecular searcher from logic computing network based on Eu (III) functionalized UMOFs for environmental monitoring. *Adv. Funct. Mater.* **2017**, *27*, 1700247.

(40) Hao, J. N.; Niu, D.; Gu, J.; Lin, S.; Li, Y.; Shi, J. Structure engineering of a lanthanide-based metal–organic framework for the regulation of dynamic ranges and sensitivities for pheochromocytoma diagnosis. *Adv. Mater.* **2020**, 2000791.

(41) Su, Y.; Yu, J. H.; Li, Y. B.; Phua, S. F. Z.; Liu, G. F.; Lim, W. Q.; Yang, X. Z.; Ganguly, R.; Dang, C. O.; Yang, C. L.; Zhao, Y. L. Versatile bimetallic lanthanide metal-organic frameworks for tunable emission and efficient fluorescence sensing. *Commun. Chem.* **2018**, *1*, 1-13.

(42) Mi, X. N.; Sheng, D. F.; Yu, Y. E.; Wang, Y. H.; Zhao, L. M.; Lu, J.; Li, Y. W.; Li, D. C.; Dou, J. M.; Duan, J. G.; Wang, S. Tunable light emission and multiresponsive luminescent sensitivities in aqueous solutions of two series of lanthanide metal–organic frameworks based on structurally related ligands. *ACS Appl. Mater. Interfaces* **2019**, *11*, 7914-7926.

(43) Li, X. J.; Zhou, S. Y.; Lu, S.; Tu, D. T.; Zheng, W.; Liu, Y.; Li, R. F.; Chen, X. Y. Lanthanide metal–organic framework nanoprobes for the in vitro detection of cardiac disease markers. *ACS Appl. Mater. Interfaces* **2019**, *11*, 43989-43995.

(44) Li, Y. Temperature and humidity sensors based on luminescent metal-organic frameworks. *Polyhedron* **2020**, *179*, 114413-114445.

(45) Cui, Y. J.; Zhu, F. L.; Chen, B. L.; Qian, G. D. Metal–organic frameworks for luminescence thermometry. *Chem. Commun*. **2015**, *51*, 7420-7431.

(46) Chen, L.; Ye, J. W.; Wang, H. P.; Pan, M.; Yin, S. Y.; Wei, Z. W.; Zhang, L. Y.; Wu, K.; Fan; Y. N.; Su, C. Y. Ultrafast water sensing and thermal imaging by a metal-organic framework with switchable luminescence. *Nat. Commun.* **2017**, *8*, 1-10.

(47) Zhang, K.; Xie, X. J.; Li, H. Y.; Gao, J. X.; Nie, L.; Pan, Y.; Xie, J.; Tian, D.; Liu, W. L.; Fan, Q. L.; Su, H. Q.; Huang, L.; Huang, W. Highly water-stable lanthanide-oxalate MOFs with remarkable proton conductivity and tunable luminescence. *Adv. Mater.* **2017**, *29*, 1701804.

(48) Gao, Y.; Jing, P. T.; Yan, N.; Hilbers, M.; Zhang, H.; Rothenberg, G.; Tanase, S. Dual-mode humidity detection using a lanthanide-based metal–organic framework: towards multifunctional humidity sensors. *Chem. Commun.* **2017**, *53*, 4465-4468.

(49) Zhou, Y.; Zhang, D.; Xing, W.; Cuan, J.; Hu, Y.; Cao, Y.; Gan, N. Ratiometric and turn-on luminescence detection of water in organic solvents using a responsive europium-organic framework. *Anal. Chem.* **2019**, *91*, 4845−4851.

(50) Yang, X. Q.; Zou, H.; Sun, X. W.; Sun, T. Y.; Guo, C.; Fu, Y. Q.; Wu, C. M. L.; Qiao, X. S.; Wang, F. One-step synthesis of mixed lanthanide metal–organic framework films for sensitive temperature mapping. *Adv. Optical Mater.* **2019**, *7*, 1900336.

(51) Zhu, Y. J.; Wang, L.; Chen, X. D.; Wang, P. C.; Fan, Y.; Zhang, P. 3D lanthanide metal-organic frameworks constructed from 2, 6-naphthalenedicarboxylate ligand: synthesis, structure, luminescence and dye adsorption. *J. Solid State Chem.* **2017**, *251*, 248-254.

(52) Hao, J. N.; Yan, B. Amino-decorated lanthanide(Ⅲ) organic extended frameworks for multi-color luminescence and fluorescence sensing. *J. Mater. Chem. C* **2014**, *2*, 6758-6764.

(53) Sun, T. C.; Wang, P.; Fan, R. Q.; Chen, W.; Hao, S.; Yang, Y. L. Functional microscale single-phase white emission lanthanide MOF for tunable fluorescent sensing and water quality monitoring. *J. Mater. Chem. C* **2019**, *7*, 3598-3606.

(54) Committee, A. M. Recommendations for the definition, estimation and use of the detection limit. *Analyst* **1987**, *112*, 199-204.

(55) Zhou, S.; Zheng, W.; Chen, Z.; Tu, D.; Liu, Y.; Ma, E.; Li, R.; Zhu, H.; Huang, M.; Chen, X. Dissolution-enhanced luminescent bioassay based on inorganic lanthanide nanoparticles. *Angew. Chem. Int. Ed.* **2014**, *53*, 12498-12502.

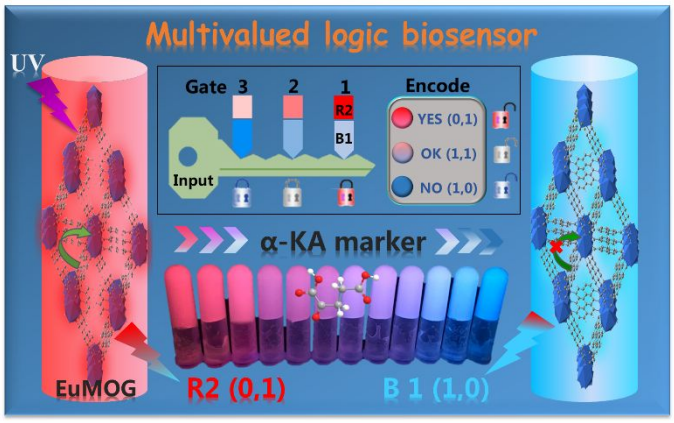
Multivalued logic biosensor
UV
Gate 3 2 1
R2
B1
Input
Encode
YES (0,1)
OK (1,1)
NO (1,0)
α-KA marker
EuMOG
R2 (0,1)
B 1 (1,0)